>

Robust Helipad Detection Algorithm (January 2007)

G. F. Nsogo, K. Kith, B. J. van Wyk and M.A. van Wyk

French South African Technical Institute in Electronics
Tshwane University of Technology, Pretoria, South Africa
nsogof@yahoo.fr, kimcheng.kith@fsatie.ac.za, vanwykb@tut.ac.za, vanwykMA1@tut.ac.za

Abstract—The design of a robust helipad detection algorithm for a small unmanned helicopter is presented. A novel Normalized Wavelet Descriptor (NWD) is proposed for invariant helipad detection. The performance of the NWD is compared to the performances of geometric moments and the Fourier descriptor using a helipad image database.

Index Terms—Robust Helipad Detection

I. Introduction

Vision is one of the most used human senses and it is therefore not uncommon for engineers to use vision-based methodologies in the design of robots and Unmanned Aerial Vehicles (UAVs) [1]. During recent years considerable resources were devoted to the design and operation of UAVs. Since the first powered flight, researchers strived to produce smaller aircraft. This goal was made possible by the miniaturization of electronic devices and the progress of new technologies.
Today Micro Air Vehicles (MAVs) that are entirely automated for take off, flight and landing is a reality. Equipped with a small and light embedded video camera and a data transmitter unit, UAVs and MAVs can be used for surveillance and monitoring without endangering the lives of human pilots. The applications of such UAVs are diverse, ranging from scientific exploration (monitoring natural disasters, forest fires, and reconnaissance) and data collection (power line multi-spectral image recording for offline fault analysis [2], chemical radiation zone monitoring or monitoring volcanic activities) to military reconnaissance and intelligence gathering (battlefield reconnaissance and spying) [3]. In all these cases the use of UAVs presents a huge potential both in terms of cost and operational capabilities.

In this paper the focus is on the design of a robust helipad detection algorithm for small unmanned air vehicles. A novel Normalized Wavelet Descriptor (NWD) is proposed and compared to geometric moments and the Fourier Descriptor (FD).

The paper outline is as follows: Related work and assumptions are presented in section 2. Pre-processing stages are introduced in section 3. Section 4 introduces the geometric moments, the FD and NWD. Experimental results are given in section 5, and finally the conclusion follows in section 6.

II. Related Research

Object recognition is central to machine vision algorithm for UAVs. Omead Amidi [4] developed a tracking method to detect the position of a ground target. The use of a high speed image template matching allowed for the detection of the helicopter's position relatively to the target. Davison [5] proposed the SLAM algorithm to detect the position of a moving camera relative to a pre-defined image by analyzing image features such as corners, lines and dots.
Burleson et al. [6] on the other hand described how vision on a helicopter can be used for an autonomous remote mission. Kehoe et al. [7] used computer vision for the autonomous control of a MAV (Micro Air Vehicle). They were able to estimate the attitude of the aircraft and target position using image processing techniques. Sharp et al. [8] also proposed an algorithm for the landing of an unmanned aerial vehicle. The proposed method is based on the extraction of target features such as corners, lines and correspondence matching.

Saripalli et al. [3] proposed the autonomous control of an aerial vehicle using a vision-based navigation system. In work closely related to ours Saripalli et al. implemented a vision based landing algorithm for an autonomous helicopter. Geometric moment descriptors were used to detect a helipad. Since geometric moments were found not to be sufficiently robust for helipad detection, this paper introduces the Normalized Wavelet Descriptor (NWD) and compares the performance of the NWD to the performances of FD and geometric moments. The method presented here differs from the preceding approaches in several ways: The threshold value is obtained automatically for each image. Edge features are

1-4244-0987-X/07/$25.00 ©2007 IEEE.

>

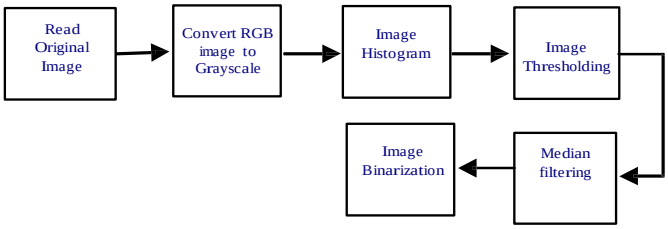

Fig. 1 Sequence of Image Processing operations performed in the preprocessing of the images

used for the helipad, and the algorithms developed can be used for most types of landing targets and is not only restricted to helipads.

Assumptions:

To extract the target from the background is a difficult task. To delimit the focus of the work and to remove some of the difficulties we made the following assumptions:

#1 We assumed that the shape of the target is known. (Any standard letter can be used, but we preferred a white H, which is a standard letter for helipad (Refer to Fig 2a).

#2 As in previous work, a sufficiently high contrast between the target and the background is assumed.

#3 It is assumed that the target is stationary and flat on the ground.

III. PREPROCESSING

The image processing steps performed in the preprocessing [9] of images in this work are described in Fig. 1.

A. Features acquisition

For the helipad algorithm, the first step involves the acquisition of our input image containing an aerial view of the helipad (Refer to Fig. 2a). The RGB image is converted into a grayscale image (Refer to Fig. 2b), using

$$Y = 0.2989 \times R + 0.5870 \times G + 0.1140 \times B. \quad (1)$$

The conversion yields an input image represented as a 2D discrete matrix Y, of dimension $R \times C$, where R is the number of rows and C is the number of columns.

Image thresholding is performed to produce an image with different regions of interest. The basic idea underlying this step is to facilitate the separation of the object of interest

Fig. 2a Image in RBG

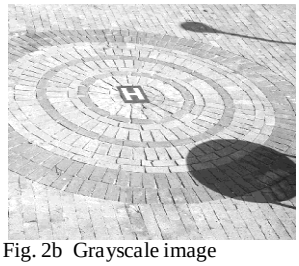

Fig. 2b Grayscale image

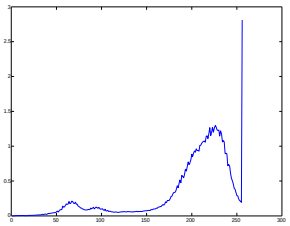

Fig. 3a Intensity distribution

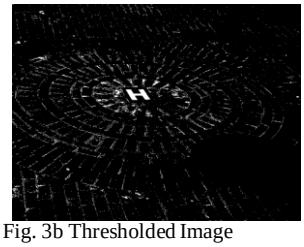

Fig. 3b Thresholded Image

(landing target) from the background. Since all the images present in our database do not share common characteristics, we cannot apply the same threshold value N, to all of them. The choice of N depends of factors such as light intensity, camera orientation, and background color. An undesirable threshold value, can cause the target disappear from the image. The image histogram represents the distribution of intensities of the grayscale image and was used to determine an appropriate value for N (Refer to Fig. 3a).

Finally, the image obtained after thresholding is converted into a binary image. The result of that digitalization is shown in Fig. 3b. For tests performed on the images in our database $200 \leq N < 255$.

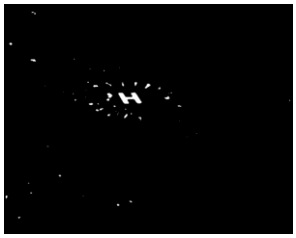

Fig. 4a Filtered Image

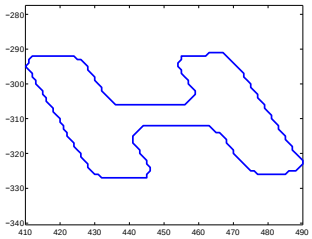

Fig. 4b Helipad detected image

B. Image Filtering and Target extraction

After the image thresholding has been performed, a noisy binary image is obtained. Image filtering was performed to decrease the amount of noise. A 9×9 median filter was applied to the input image. Each output pixel is set to the average of the value in the neighborhood of the corresponding input pixel. The resulting image is then converted into a binary image as the one shown in Fig. 4a.

After image filtering has been performed, it is common to have an output image composed of the region of interest and residual noise. The extraction of the target begins with the definition of an inclusive rectangle. We predefined the size of that rectangle to (nlR, ncR) where nlR represent the number of rows and ncR the number of columns. The size of inclusive rectangle corresponds to the size of the smallest helipad that the algorithm can detect. The image is scanned row wise in order to determine the number of objects remaining after the image has been filtered.

Each remaining object is compared to the size of the inclusive rectangle. An object with a size smaller than the rectangle is discarded. The shape is extracted using an 8-neighborhood tracing technique in boundary coordinates (Refer to Fig. 4b).

>

IV. INVARIANT MOMENTS

A. Geometric Moments

The use of geometric moments to analyze and identify an image has been proposed by Hu [10]-[11]. Geometric moments can provide sufficient information about the target to be reconstructed from its moments.

Assume that the extracted target is a piecewise continuous function f(x,y). Then its geometric moment of order p+q is defined as

$$m_{pq} = \int_{-\infty}^{\infty}\int_{-\infty}^{\infty} x^p y^q f(x,y)\,dxdy \qquad p,q = 0,1,2,3,.... \tag{2}$$

The $(p+q)^{th}$ order moment of an image I(x,y), where I(x,y) is a discrete function, is given by

$$m_{pq} = \sum_i \sum_j I(i,j) i^p j^q, \tag{3}$$

with $i = 0,1\ldots N_x - 1$, $j = 0,1,\ldots..N_y - 1$; Here i, j correspond respectively to row and column number of pixel I(i,j). The central moments of order p+q of a two dimensional shape represented by function f(x, y) are given by

$$\mu_{pq} = \int_{-\infty}^{\infty}\int_{-\infty}^{\infty} f(x,y)(x-\bar{x})^p (y-\bar{y})^q dxdy, \tag{4}$$

where the center of gravity of the object is defined by

$$\bar{x} = \frac{m_{10}}{m_{00}}, \qquad \bar{y} = \frac{m_{01}}{m_{00}}. \tag{5}$$

The central moment can therefore also be given by

$$\mu_{pq} = \sum_i \sum_j I(i,j)(i-\bar{x})^p (j-\bar{y})^q \tag{6}$$

The normalized central moment η_{pq} is given by

$$\eta_{pq} = \frac{\mu_{pq}}{\mu_{00}^{\gamma}}, \quad \gamma = \frac{p+q+2}{2}, \tag{7}$$

for p+q = 2, 3, 4… It can be shown that the central moments up to third order are given by the following relations [3]-[10]

$$\mu_{00} = m_{00} = \mu \tag{8}$$
$$\mu_{10} = \mu_{01} = 0 \tag{9}$$
$$\mu_{20} = m_{20} - \mu.^2(\bar{x}) \tag{10}$$
$$\mu_{11} = m_{11} - \mu.(\bar{x}).(\bar{y}) \tag{11}$$
$$\mu_{02} = m_{02} - \mu^2.(\bar{y}) \tag{12}$$
$$\mu_{30} = m_{30} - 3m_{20}.(\bar{x}) + 2\mu^3.(\bar{x}) \tag{13}$$
$$\mu_{21} = m_{21} - m_{20}.(\bar{y}) - 2m_{11}.(\bar{x}) + 2\mu.^2(\bar{x}).(\bar{y}) \tag{14}$$
$$\mu_{12} = m_{12} - m_{02}.(\bar{x}) - 2m_{11}.(\bar{y}) + 2\mu.^2(\bar{x}).(\bar{y}) \tag{15}$$
$$\mu_{03} = m_{03} - 3m_{02}.(\bar{y}) + 2\mu.^3(\bar{y}) \tag{16}$$

The following sets of invariant moments Φ1 to Φ7 are obtained from the central moment:

for $p+q = 2$:

$$\Phi_1 = \eta_{20} + \eta_{02} \tag{17}$$
$$\Phi_2 = (\eta_{20} + \eta_{02})^2 + 4\eta_{11}^2 \tag{18}$$

for $p+q = 3$

$$\Phi_3 = (\eta_{30} - 3\eta_{12})^2 + (\eta_{03} - 3\eta_{21})^2 \tag{19}$$
$$\Phi_4 = (\eta_{30} + \eta_{12})^2 + (\eta_{03} + \eta_{21})^2 \tag{20}$$

$$\Phi_5 = (\eta_{30} - 3\eta_{12})(\eta_{30} + \eta_{12})[(\eta_{30} + \eta_{12})^2 - 3(\eta_{21} + \eta_{03})^2] + (\eta_{03} - 3\eta_{21})(\eta_{03} + \eta_{21})[(\eta_{03} + \eta_{21})^2 - 3(\eta_{12} + \eta_{30})^2] \tag{21}$$

$$\Phi_6 = (\eta_{20} - \eta_{02})[(\eta_{30} + \eta_{12})^2 - (\eta_{21} + \eta_{03})^2] + \eta_{11}(\eta_{30} + \eta_{12})(\eta_{21} + \eta_{03}) \tag{22}$$

$$\Phi_7 = (3\eta_{21} - \eta_{03})(\eta_{30} + \eta_{12})[(\eta_{30} + \eta_{12})^2 - 3(\eta_{21} + \eta_{03})^2] + (\eta_{30} - 3\eta_{12})(\eta_{21} + \eta_{03})[(\eta_{03} + \eta_{21})^2 - 3(\eta_{30} + \eta_{12})^2] \tag{23}$$

The computation of the eccentricity (i.e. ratio of the length of major axis to the length of minor axis) is a function of the angle generated by the object's orientation (major axis of the object) and the x-axis. The object orientation is obtained via θ as

$$\theta = \frac{1}{2}\arctan\left(\frac{2\mu_{11}}{\mu_{20} - \mu_{02}}\right). \tag{24}$$

The eccentricity (ε) is also invariant to scaling, rotation, and translation. It is computed as

$$\varepsilon = \left[\frac{\mu_{02}\cos^2\theta + \mu_{20}\sin^2\theta - \mu_{11}\sin 2\theta}{\mu_{02}\sin^2\theta + \mu_{20}\cos^2\theta - \mu_{11}\cos 2\theta}\right]^2. \tag{25}$$

B. Fourier Descriptor (FD) Method

Performance of the FD obtained from the representation by the centroid distance signature is superior to other FDs (Zhang et al [12]). This result was confirmed by Kith [13].
The centroid, (x_c, y_c), and the contour signature represented by the distance of the point on the contour to the centroid is calculated such as

$$x_c = \frac{1}{n}\sum_{i=1}^{n} x_i, \qquad y_c = \frac{1}{n}\sum_{i=1}^{n} y_i \tag{26}$$

$$\text{and} \qquad r_i = \sqrt{((x_i - x_c)^2 + (y_i - y_c)^2)} \tag{27}$$

The centroid distance signature r_i, is invariant to translation. The Fourier transformation is applied to the contour signature of the extracted helipad to obtain the Fourier coefficients a_k [9-13] given by

$$a_k = \frac{1}{n}\sum_{i=1}^{n} r_i \exp(-j2\pi ki/n). \tag{28}$$

From this definition, we can show that

$$a_k = s\exp(jk\tau/n) * \exp(j\Phi) a_k^{(0)}, \quad k \neq 0 \tag{29}$$

>

a_k^0 and a_k respectively represent the Fourier coefficients of the contour signature of the reference helipad (the reference landing to which all other target will be compared) and the equivalent transformed helipad. Here exp(jkτ), exp(jΦ) and s are the terms due to changes on the reference helipad (rotation and scaling) [14].

All the Fourier coefficients appear not to be affected by the translation except for a_0 .If we define

$$b_k = \frac{a_k}{a_0} \tag{30}$$

where a_k is defined in equation (29), we obtain:

$$b_k = \exp(jk\tau) b_k^0, \tag{31}$$

where b_k and b_k^0 respectively are normalized Fourier coefficients of the transformed contour and the original contour.

C. Normalized Wavelet Descriptor (NWD) Method.

Let r(t) be the contour signature. The Continuous Wavelet Transform (CWT) of r(t), by the wavelet function ψ, is defined as

$$C_{\psi,r}(b,a) = \frac{1}{a} \int_R r(t) \psi^* \left(\frac{t-b}{a} \right) dt, \tag{32}$$

where $b \in R$ represents the shifting parameter, while $a > 0$ defines the dilation parameter of the wavelet transform. The analyzing wavelet $\psi(t)$ must have a null DC component, which is known as the simplified admissibility condition. The CWT presents many useful and desirable properties for a shape analysis scheme [10]. For example from the equation (32), if s(t) = r(t-τ), one can show that

$$C_{\psi,s}(b,a) = C_{\psi,r}(b-\tau,a). \tag{33}$$

This means that if we shift or translate the contour signature r(t) by τ, the resulting CWT coefficients is the τ translation of the CWT coefficients of r(t).

In many applications, the signal or the data to be processed is discrete. In such cases, the discrete wavelet transform (DWT) instead of the CWT should be used. The DWT convolves the shape signature with a low-pass filter and a high-pass filter followed by dyadic decimation (down sampling) to obtain the approximation and detail coefficients respectively for the first level of decomposition. This procedure is repeated for all subsequent levels of decomposition, except that the shape signature is replaced by the approximation coefficients from the previous level. The drawback of the DWT compared to the CWT is that the equality of equation (33) is not valid. To overcome this problem, we fix the starting point on the shape contour such that two similar (according to translation, rotation and scale) contours have the same starting point, before applying the DWT. In our implementation, a point on the contour is chosen as the starting point if the distance from the point to the centroid of the contour has a maximum value.
Another problem with the DWT is related to convolution. As usual, when a convolution is performed on finite-length signals, border distortions arise. Various methods are available to deal with this problem. Since in our case the helipad contour is a closed curve, the best solution is to use the periodic extension.
At this stage, after having fixed the starting point on the contour and applying the DWT to the contour signature, the wavelet coefficients are invariant to contour translation and rotation. To be invariant to scale, we have to normalize the wavelet coefficients by the energy of the shape signature. This normalization yields the NWD. The summary of the algorithm is presented in the Table 1.

Table 1: NWD algorithm

NWD extraction algorithm
1: Preprocessing (section 2) 2: Choose the point on the contour that has maximum distance from the centroid as starting point 3: Calculation the approximation coefficients at level L-3 of discrete wavelet transform. (L is the maximum level of decomposition of the contour signature) 4: Normalize these coefficients according to the energy of contour signature

V. EXPERIMENTAL RESULTS

To test the different methodologies, tests were performed on images included in a TUT helipad database, containing 153 images. The preprocessing phase was successful for 151 images, given a success rate of 98.7%. This simply implies that an object similar in size to a helipad has been detected.

The second phase of the experiment was to determine if the detected object indeed is a helipad. The invariance of the three descriptors to translation, rotation and scaling therefore had to

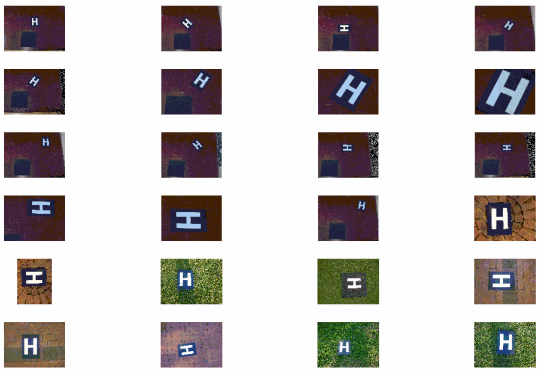

Fig. 5 Tested images present in the database

be assessed. Tests were preformed on a subset of 23 images shown in Fig. 5.

>

The image in the first row, first column was used as the reference image or object. Other images are transformed versions of this image (translated, rotated and scaled). By definition, if the descriptor of the reference image is represented by a vector of coefficients a = (a_1, …, a_l) and the descriptor of an image in the database by a vector of coefficients b = (b_1, …, b_l), the city-block distance between these a and b is defined as

$$d(a,b) = \sum_{i=1}^{l} |a_i - b_i|, \quad (34)$$

where l is the dimension of the descriptors (number of coefficient calculated). Ideally d(a,b) between the reference image and all the other images in the database should be zero.

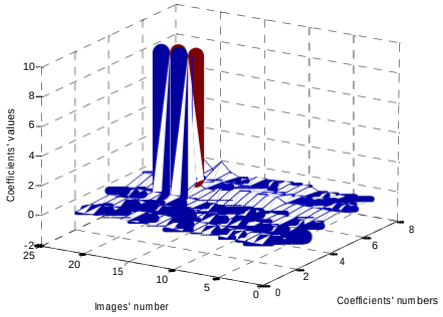

Fig. 6 Plot of Invariant Moment coefficients

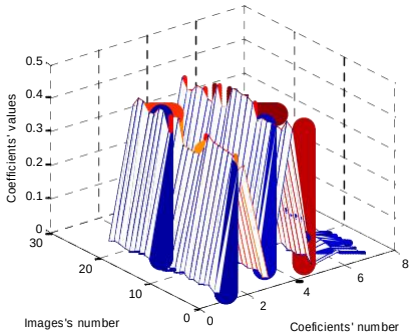

Fig. 7 Plot of Fourier descriptor coefficients

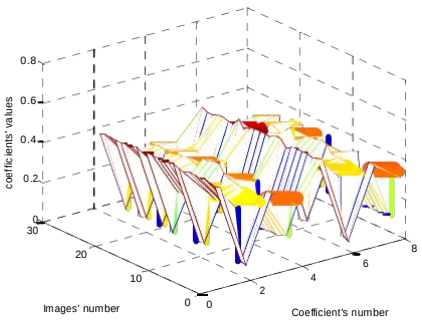

Fig. 8 Plot of Wavelet descriptor coefficients

Table 1 represents the similarity measure between the descriptor of the reference image and the descriptor of the 23 other images in the database using the city block distance.

Table 1 Comparative table of descriptor efficiency

Image number	Fourier Descriptor City block distance	Invariant Moment City block distance	Normalise Wavelet Descriptor City block distance
image1	0.06511	0	0.349816
Image2	0.126263	0	0.341438
Image3	0.048904	0	0.028053
Image4	0.025715	0	0.029647
Image5	0.037264	0	0.026271
Image6	0.021405	0	0.031122
Image7	0.033139	0	0.028351
Image8	0.021605	0.554059	0.328435
Image9	0.094404	0.554059	0.346731
Image10	0.153361	0.554059	0.128688
Image11	0.146541	0.554059	0.114832
Image12	0.155649	0.554059	0.109343
Image13	0.141106	0.554059	0.107568
Image14	0.029011	0.554059	0.333837
Image15	0.05423	0	0.022014
Image16	0.094404	0	0.346731
Image17	0.05423	0.554059	0.022014
Image18	0.05423	9.61767	0.022014
Image19	0.046043	0.554059	0.313145
Image20	0.046043	9.61767	0.313145
Image21	0.05423	0.554059	0.022014
Image22	0.05423	0.554059	0.022014
Image23	0.046043	0.554059	0.313145

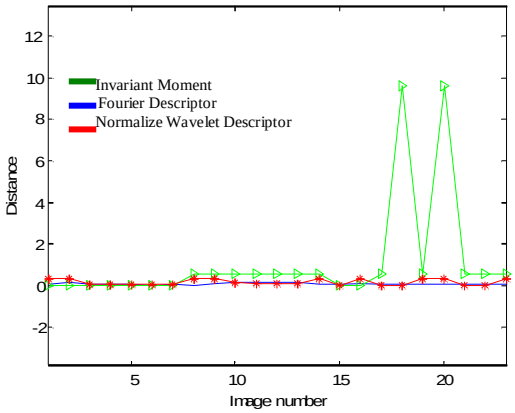

Fig. 9 Comparative graph of descriptor efficiency

Among the tested descriptors, the best one is the one with the lowest mean and variance (Refer to Table 2). The results obtained from the invariant moment are encouraging but are clearly not robust enough. It is clear that the FD is more robust than both the geometric moment and the NWD. Note that the NWD significantly outperformed the moment descriptor.

Table 2 Mean and variance table

Methods	Mean	Variance
Invariant moment	1.1254	7.2524
FD	0.0697	0.0020
NWD	0.1609	0.0208

The final phase of the experiment was to verify the algorithm's behavior in case of non helipad detection using a database (TUT_Helipad2) containing both helipad H and non helipad objects. The first contour in Figure 10a, represents the request contour. The city-block distance d(a,b), between request shape, and each shape in the database is evaluated to measure the similarity between the requested shape and the shape in the database. This means that the smaller d(a,b), the closer it is to the request (Display order of the shape, is in according to the distance d(a,b)) (see Fig. 10).

>

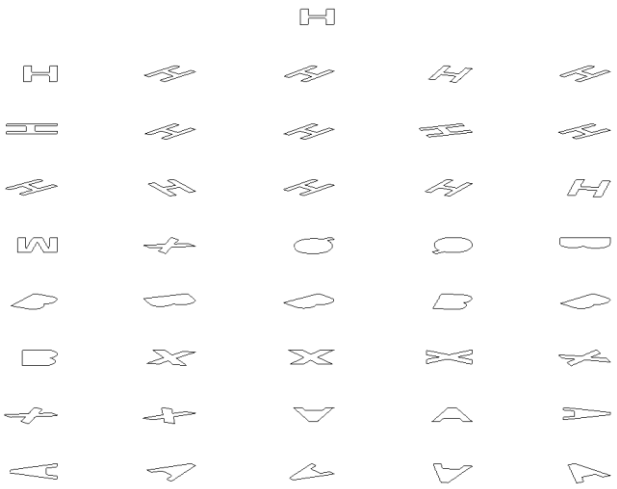

Fig. 10 Helipad validation

The similarity between the requested image and other images in the database corresponds to the distance on the ordered similarity plot (see Fig. 11).

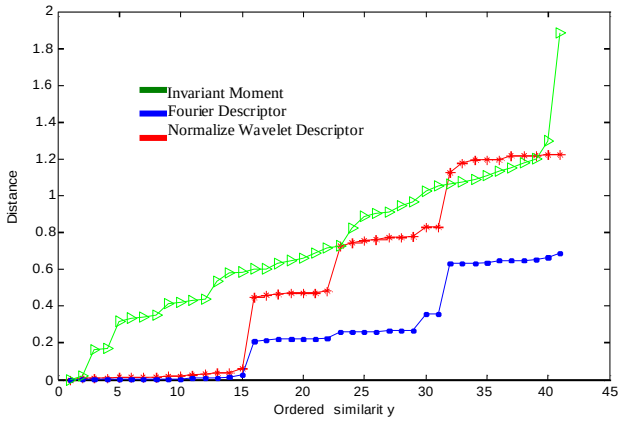

Fig. 11 Ordered similarity plot

VI. Conclusion

In this paper the design of a robust helipad detection algorithm for a small unmanned helicopter was presented. A novel Normalized Wavelet Descriptor (NWD) was proposed for invariant helipad detection. The performance of the NWD was compared to the performances of the geometric moment and the Fourier Descriptor (FD) using a helipad image database. Experimental results show that the NWD has potential, but that FD performed the best.

More extensive testing and algorithm refinement is planned as part of the further work.

References

[1] Jean-Christophe Zufferey, "Bio-Inspired Visiom-Based Flying Robots" Ph. D, thesis N° 3195, faculty of Sciences and Engineering Technics, Ecole Polytechnique Federal de Lausane, February 2005.

[2] R Stolper, Jaco Hart, and N Mahatho, "The design and evaluation of a Multi-Spectral Imaging Camera for the inspection of transmission lines and substation equipment", CSIR, 2005.

[3] Srikanth Siripalli, James F. Montgomery, and Gaurav S. Sukhatme in "Vision based autonomous landing of an unmanned Aerial Vehicle", IEEE international conference on Robotics and Automation, May 2002.

[4] AMIDI O, "An Autonomous Vision-Guided Helicopter", Ph. D. thesis, Robotics Institute, Carnegie Mellon University, ch. 2, August 1996.

[5] Andrew J. Davidson, in "Real time simultaneous location and mapping with a single camera".

[6] Walter L. Burleson, Kristopher Keller and John F. Sweigart in "Polytechnic Autonomous Remote Reconnaissance System (SPARRS-2002)", in International Aerial Robotics Competition, 2001 – 2004 matched filters.

[7] Joseph J. Kehoe, Ryan Causey, Rick Lind and Andrew J. Kurdila, in "Maneuvering and Tracking for a Micro Air Vehicle using Vision-Based Feedback", Department of Mechanical and Aerospace Engineering, University of Florida, SAE International, 2004.

[8] Courtney S. Sharp Omid Shakernia S. Shankar Sastry, "A Vision System for Landing an Unmanned Aerial Vehicle", Department of Electrical Engineering & Computer Science, University of California Berkeley, California, 94720.

[9] R. O. Duda, P. E. Hart, D. G. Stork, " Pattern Classification ", 2nd ed. Canada: John Willey, 2001, pp. 1-18

[10] Luciano da Fountoura Costa, Roberto M. Cesar Jr., " Shape Analysis and Classification ", CRC Press LLC Ed. , pp 291-298.

[11] Sergios Theodorus, Konstantinos Koutroumbas, " Pattern Recognition ", San Diego, Academic Press, Ed, 1998, pp. 245-248, 259-262.

[12] Dengsheng Zhang and Guojun Lu, Study and evaluation of different Fourier methods for image retrieval, Image and Vision Computing, 23 (2005) 33-49.

[13] Kimcheng Kith, Barend J. van Wyk, Michael A. van Wyk, "The Normalized Wavelet Descriptor for Shape Recognition", "submitted for publication" to International Journal of Wavelets, Multiresolution and Information Processing, October 3, 2006.

[14] Kimcheng KITH, "Contribution a la description des formes par la transformation en ondelettes", PhD thesis, Universit´e de La Rochelle, 2005.

Copyright Information